Journal of Engineering Science and Technology
Vol. 14, No. 5 (2019) 2552 - 2564

THE EFFECT OF CHANNEL WIDTH ON BIOMETRIC FLOW FIELD TOWARDS PERFORMANCE OF POLYMER ELECTROLYTE MEMBRANE FUEL CELL

A'RASY FAHRUDDIN[1,2,*], DJATMIKO ICHSANI[1], FADLILATUL TAUFANY[3], BUDI UTOMO KUKUH WIDODO[1]

[1]Mechanical Engineering Department, Institut Teknologi Sepuluh Nopember (ITS), Jl. Raya ITS, Keputih, Sukolilo, 60111, Surabaya, Indonesia
[2]Mechanical Engineering Department, Universitas Muhammadiyah Sidoarjo, Jl. Raya Gelam No.250, 61271, Sidoarjo, Indonesia
[3]Chemical Engineering Department, Institut Teknologi Sepuluh Nopember (ITS), Jl. Raya ITS, Keputih, Sukolilo, 60111, Surabaya, Indonesia
*Corresponding Author: arasy.fahruddin@umsida.ac.id

Abstract

In this paper, we apply a biometric flow field design, not just as an attractive design, but also as a promising concept, that provides high electrical performance, with low-pressure drop. The purpose of this study was to study the effect of the channel width of biometric flow fields on the performance of the Polymer Electrolyte Membrane Fuel Cell. Numerical simulations have been done using Ansys Fluent software. 9-layer 3D model has been made with 25 cm² active cell area. Biometric flow fields are used on the cathode side and apply Murray Law as a reference, while the anode side uses a single serpentine flow field. Channel width varies by 1 mm; 1.25 mm; and 1.5 mm. The results show that the 1.25 mm channel width produces higher current density and lower pressure drop than other width at low to medium voltage. When compared to conventional flow fields, biometric flow field designs can produce higher power density up to 22%.

Keywords: Biometric flow field, Channel width, Polymer electrolyte membrane fuel cell.

1. Introduction

A fuel cell is an energy conversion engine that produces electricity from the results of electrochemical fuel reactions [1]. Because it uses fuel, the fuel cell does not take a long time for the charging process like a battery. Polymer Electrolyte Membrane Fuel Cell (PEMFC) is one type of fuel cell that uses hydrogen as its fuel, making it more environmentally friendly because it only produces exhaust gas in the form of water vapour [2]. PEMFC works at a relatively low temperature, therefore, it can be applied to a variety of portable equipment including the supply of electrical energy in light transport equipment. Like other types of fuel cells, fuel supply at PEMFC will affect its performance. In addition, the fuel supply to the reaction area is strongly influenced by the flow field design used [3, 4].

Chowdhury et al. [5] have examined the channel width ratio with the width of the land. The results of his research show that the narrower the channel, the pressure drop and the current density will increase. However, the research is limited to a single straight channel. Other researchers have also examined the effect of channel width on PEMFC performance [6-8] and shows that the channel width greatly affects the pressure drop and current density.

Currie [9] has researched several flow field designs on the cathode side to determine their effect on PEMFC performance. From several forms of the flow field, finally the biometric and triple serpentine forms were chosen to be compared. This research shows that PEMFC performance with biometric flow field can be improved by applying Murray Theory. PEMFCs with biometric flow fields produce a slightly lower current density in high current than triple serpentine because of poor drainage problems. However, the pressure drop on the biometric flow field is lower, so the power losses are lower. In addition, a high-pressure drop can trigger reactant leakage and cell damage [10]. Ozden et al. [11] has examined leaf flow field with Murray Law to be applied to Direct Methanol Fuel Cell (DMFC) and shows that the combination of the serpentine flow field on the anode side and biometric flow field on the cathode side produces the highest current density. Murray's Law was used to calculate the required parent and daughter channels diameters of bio-inspired leaf flow fields. This law reveals that the cube of the hydraulic diameter of the parent channel is equal to the sum of the cubes of the hydraulic diameters of the daughter channels. Guo et al. [12] have examined the design of the flow field bio-inspired by tree leaf using Murray law to determine the flow channel widths of different generations. The results show that the bio-inspired interdigitated designs substantially improve fuel cell performance by 20-25% compared to conventional designs. Roshandel et al. [13] have examined the design of flow field inspired by leaf and the results show that the reactant concentration on catalyst surface is more homogeneous and the power density is higher than parallel and serpentine flow channels. From several other studies, also showed that the use of a biometric flow field provides promising performance with a better pressure drop compared to conventional flow field [14, 15]. However, some research on biometric flow field offers quite complex designs, which may be difficult to make. As for simple biometric designs [11, 13], it has not been studied about the effect of channel width on cell performance.

The purpose of this study was to determine the effect of channel width on the biometric flow field on PEMFC performance and pressure drop. Branch channel width will affect the flow of mass uniformity at each point. The more uniform

the mass flow rate, the more uniform the current produced at each point, therefore, that it will increase the value of current density. In this paper, we will also discuss the comparison of leaf design proposed with conventional parallel flow fields as a consideration.

2. Numerical model

2.1. Model design and geometry

Numerical simulations are performed using the Ansys Fluent software, by calling the fuel cell PEM addon module. The model used is PEM single stack 3D fuel cell with 25 cm² membranes active area, according to previous research references [11, 12, 14]. The model consists of 9 parts, that is a pair of current collectors, a pair of reactant fluids, a pair of gas diffusion layers, a pair of catalyst layers, and a membrane [16].

Flow field biometrics are used in leaf form with variations in channel width of 1 mm; 1.25 mm; 1.5 mm. Chowdhury et al. [5] and Guo et al. [12] conducted research on this variation is based on the consideration results. The depth of the channel and the width of the rib are made constant 1 mm. The flow field design is more clearly seen in Fig. 1.

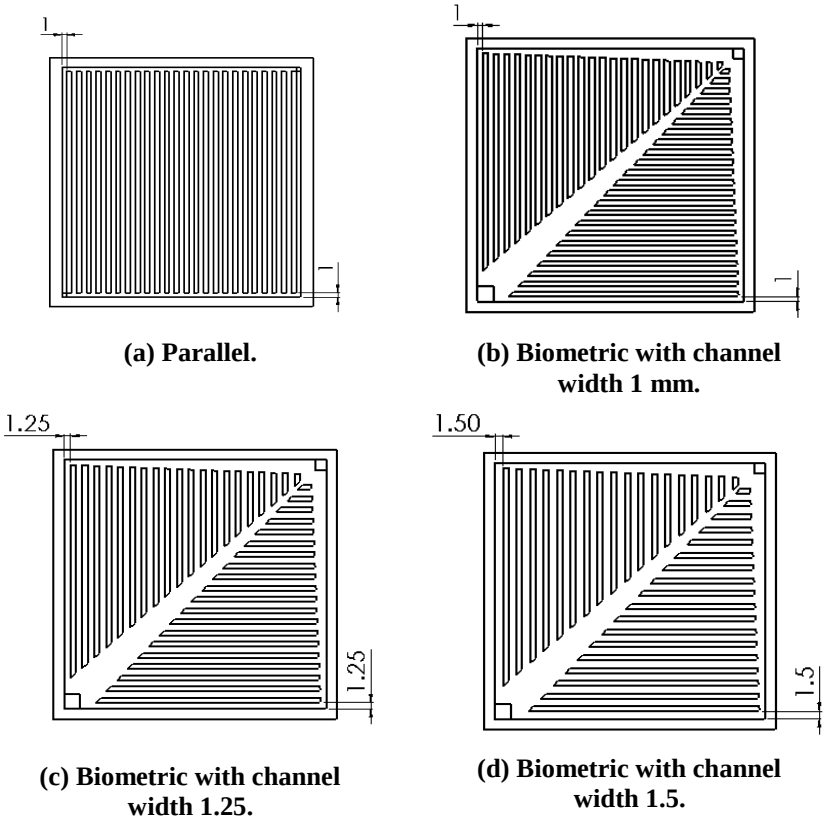

(a) Parallel.

(b) Biometric with channel width 1 mm.

(c) Biometric with channel width 1.25.

(d) Biometric with channel width 1.5.

Fig. 1. Flow field design.

The stack dimension is fully shown in Fig. 2. The full stack consists of 9 sections as described previously. The dimensions of each part are more clearly shown in Table 1, which were based on several references [17, 18].

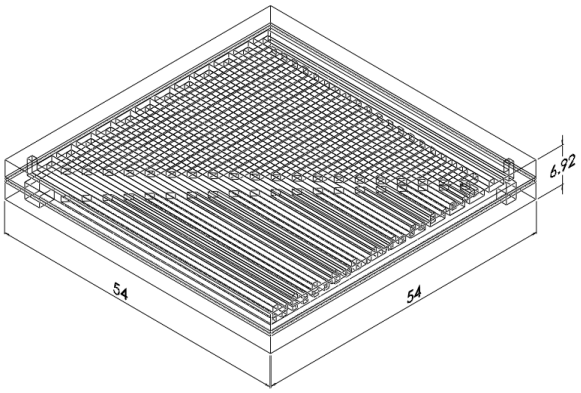

Fig. 2. Dimensions of fuel cell stack in mm.

Table 1. Model geometry.

Properties	Value	Unit
Channel height	1	mm
Diffusion layer thickness	0.42	mm
Catalyst layer thickness	0.012	mm
Membrane thickness	0.05	mm
Current collector thickness	3	mm

2.2. Model equation

In this study, the governing equation used refers to Ansys Fluent Fuel Cell Modules Manual [19]. The basic equation used is the following transport Eq. (1) [16].

$$\nabla.\left(\rho\varphi\vec{V}\right) = \nabla.\left(\Gamma_{\varphi}\nabla\varphi\right) + S_{\varphi} \tag{1}$$

where φ is the transported quantity (mass, momentum, energy), ρ is the mixture density, $\vec{V}$ is velocity vector, Γ_{φ} is diffusivity of transported quantity, and S_{φ} is the source term. Driving force electrochemical reactions that occur are potential in the solid phase and membrane phase as in Eq. (2) [16]

$$\nabla.(\sigma_S\nabla\phi_S) = -R_S\,; \quad \nabla.(\sigma_m\nabla\phi_m) = -R_m \tag{2}$$

where σ is electrical conductivity, ϕ is potential, and R is an electrical current, while s and m are solid and membrane phase. For solid-phase, $Rs = -Ra$ on the anode side, $Rs = +Rc$ on the cathode side. As for the membrane phase $Rm = +Ra$ on the anode side and $Rm = -Rc$ on the cathode side. Ra and Rc obtained the Butler-Volmer equation as follows [19]

$$R_a = \zeta_a j_a^{ref}\left(\frac{[H_2]}{[H_2]_{ref}}\right)^{\gamma_a}\left(e^{\frac{\alpha_a F\eta_a}{RT}} - e^{-\frac{\alpha_c F\eta_a}{RT}}\right) \tag{3}$$

$$R_c = \zeta_c j_c^{ref}\left(\frac{[O_2]}{[O_2]_{ref}}\right)^{\gamma_c}\left(-e^{\frac{\alpha_a F\eta_c}{RT}} + e^{-\frac{\alpha_c F\eta_c}{RT}}\right) \tag{4}$$

$$\eta_a = (\phi_S - \phi_m) \quad (5)$$

$$\eta_c = (\phi_S - \phi_m - V_{OC}) \quad (6)$$

where ζ is a specific active surface area, j_{ref} is reference exchange current density per active surface area, α_a and α_c are the anodes and cathode transfers coefficients, γ_a and γ_c are anode and cathode concentration exponents, η_a and η_c are the anode and cathode overpotentials while V_{oc} is open-circuit voltage.

Uniformity of velocity shows the uniformity of oxygen supply at each point on the side of the cathode. Uniformity of oxygen supply will improve the electrochemical reactions that occur in each position. To determine the uniformity of velocity, the gamma uniformity index is used [20].

$$\gamma = 1 - \int_0^A \frac{\sqrt{(\bar{u}-u)^2}}{2.A.\bar{u}} dA \quad (7)$$

where $\bar{u}$ is the average velocity and A is the area.

2.3. Model parameter and boundary condition

The model is assumed to be a single-phase laminar flow with a working temperature of 333 K and an operating pressure of one atm. Hydrogen and oxygen flow mass as reactant gas are kept constant at 8.10^{-7} kg s^{-1} and 2.10^{-5} kg s^{-1}. While the operating voltage is varied by 0.8 V; 0.6 V; 0.4 V; and 0.2 V. Based on studies by Heidary et al. [16], Iranzo et al. [17] and Limjeerajarus and Charoen-amornkitt [18], the detailed model parameters are as shown in Table 2.

Table 2. Parameter model.

Property	Value	Unit	Reference
Density of diffusion layer	321.5	kg m^{-3}	Iranzo et al. [17]
Electric conductivity of diffusion layer	280	ohm^{-1} m^{-1}	Iranzo et al. [17]
Porosity of diffusion layer	0.6		Heidary et al. [16]
Porosity of catalyst layer	0.4		Heidary et al. [16]
Surface to volume ratio of catalyst layer	1.127×10^7	m^2 Pt m^{-3}	Heidary et al. [16]
Thermal conductivity of the membrane	0.16	Wm^{-1} K^{-1}	Iranzo et al. [17]
Dry membrane density	1980	kg m^{-3}	Iranzo et al. [17]
Anode concentration exponent	1		Heidary et al. [16]
Cathode concentration exponent	1		Heidary et al. [16]
Open circuit voltage	1.05	V	Heidary et al. [16]
Anode reference concentration	0.0008814	kmol m^{-3}	Limjeerajarus and Charoen-amornkitt [18]
Cathode reference concentration	0.0008814	kmol m^{-3}	Limjeerajarus and Charoen-amornkitt [18]
Anode charge transfer coefficient	1		Limjeerajarus and Charoen-amornkitt [18]
Anode reference current density	7.17	A m^{-2} Pt^{-1}	Limjeerajarus and Charoen-amornkitt [18]
Cathode charge transfer coefficient	1		Limjeerajarus and Charoen-amornkitt [18]
Cathode reference current density	7.17×10^5	A m^{-2} Pt^{-1}	Limjeerajarus and Charoen-amornkitt [18]

3. Results and Discussion

3.1. Model validation

For validation, with the results of experiments, Chang and Wu [21] have compared numerical simulations. In a previous study, we made a triple serpentine flow fields design simulation [22] are close to the results of experiments conducted by Chang, as shown in Fig. 3. Validation results show the appropriate tendency between the simulation results and the experimental results. Using the average percentage

difference formula [23] there is 1.5% error. Chang and Wu [21] compared the simulation method used in this study with the experiment because it shows the closest results. This simulation method has approached experimental results, therefore, this simulation method can be used for different flow field designs and different flow field sizes.

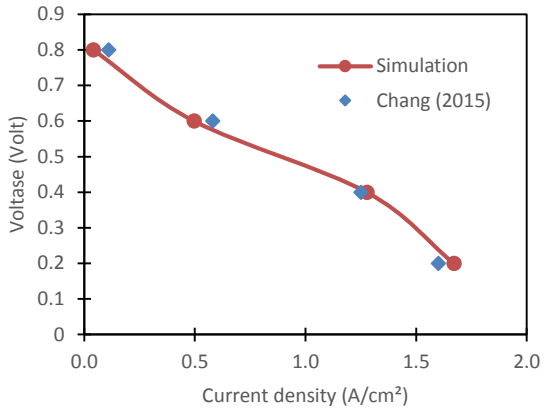

Fig. 3. Validate simulation results with experiments.

3.2. Velocity distribution in biometric and parallel flow fields

In Fig. 4, it can be seen that the oxygen velocity distribution for biometric and parallel flow fields looks different. The biometric flow field shows a more uniform velocity distribution on the branch channel than parallel. Velocity uniformity index surface integral from the fluent result report for biometric flow field with 1.25 mm channel width is 0.555, while that of the parallel flow field is 0.412. This difference in velocity distribution is caused by the branch channel angle in the biometric flow field, which is more tapered, therefore, the fluid is more easily divided into branch channels. Whereas, in parallel flow fields, branch channels are perpendicular to the main channel, therefore, in high-speed areas the fluid is difficult to turn [24]. Uniformity of fluid velocity in-branch channels shows the uniformity of mass flow of oxygen supply. The better oxygen supplies the better the cell performance.

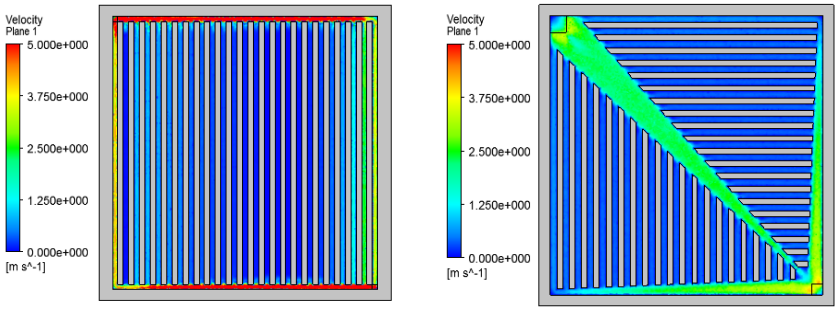

(a) Parallel flow fields. **(b) Biometric flow fields.**

Fig. 4. Distribution of oxygen velocity in cathode side.

3.3. Distribution of oxygen concentration in biometric and parallel flow fields

In Fig. 5, it can be observed that the distribution of oxygen concentration corresponds to the velocity distribution in the channel. The greater the velocity in a channel the greater the flow mass, the greater the oxygen concentration in the channel. Furthermore, the longer the channel, the lower the concentration of oxygen at the end of the channel. The oxygen velocity in the middle area of the parallel flow field is very low, so the oxygen concentration will quickly run out in the middle.

As explained by Lim et al. [23], that in conventional parallel channels the velocity will be high near the inlet and outlet. In biometric flow fields, the oxygen velocity entering each branch is almost uniform. However, oxygen continues to be consumed, therefore, in the long branches oxygen will run out at the end and the remains are the product of water vapour flowing into the outlet. To show the uniformity of oxygen concentration in the flow field, uniformity surface integral values are taken from the fluent result report according to Eq. (7). Oxygen concentration uniformity index for biometric flow field with 1.25 mm channel width is 0.632, while for parallel flow field is 0.515.

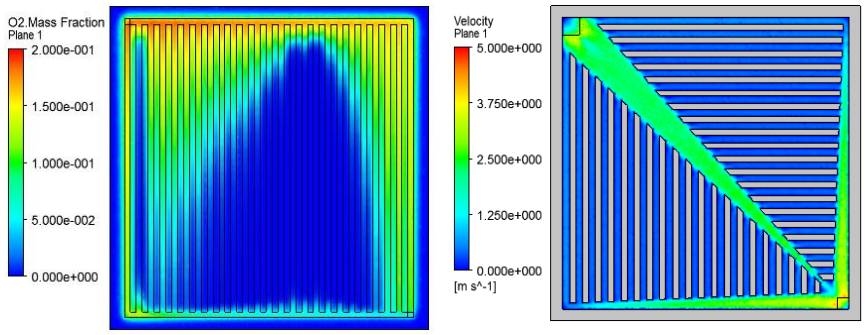

(a) Parallel flow fields. **(b) Biometric flow fields.**

Fig. 5. Distribution of oxygen concentration in cathode diffusion layer.

3.4. Current density and power density

Figure 6 shows a polarization graph that compares the biometric flow fields and conventional parallel flow fields. Figure 6 shows that the use of biometric flow fields on the cathode side shows a higher performance than parallel flow fields. This is because flow mass uniformity in the biometric flow fields is better than the parallel, therefore, the average oxygen supply on the cathode side becomes larger than the parallel flow fields.

Figure 6 also compared the influence of the branch channel width of 1 mm and 1.25 mm in the biometric flow field. From Fig. 6, it can be seen that the branch channel width does not have a significant effect on macrocell performance. However, for large power capacity, it will be necessary to consider. The effect of the width of the new channel is illustrated with a more precise scale in Figs. 7 and 8.

From Fig. 7, (at 0.4 V), it can be seen that current density is 0.825 A/cm² for 1.25 mm channel width. At 1 mm channel width, a slightly lower current density is

produced. The lowest current density is at 1.5 mm channel width. The amount of the current density is very suitable with 1.25 mm channel width. Current density is influenced by the oxygen concentration on the diffusion layer of the cathode side, the greater the oxygen concentration the greater the current density [13]. Current density is also influenced by pressure drop, the greater the pressure drop the greater the current density [5]. Narrower channels will produce a higher pressure drop but lower oxygen mass flow. Conversely, the wider the channel, the higher the oxygen mass flow, the lower the pressure drop. Adequate channel width will provide sufficient mass flow and pressure drop. At medium voltage (0.4 V), the cell does not need a lot of oxygen to react. Therefore, a wider channel is less effective at increasing current density.

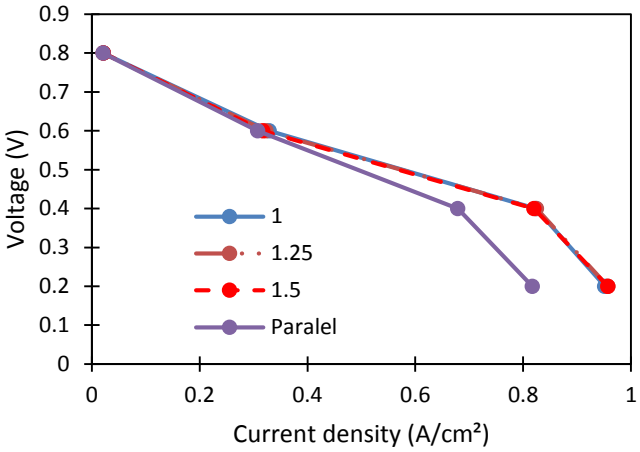

Fig. 6. Graph of polarization with variations flow fields.

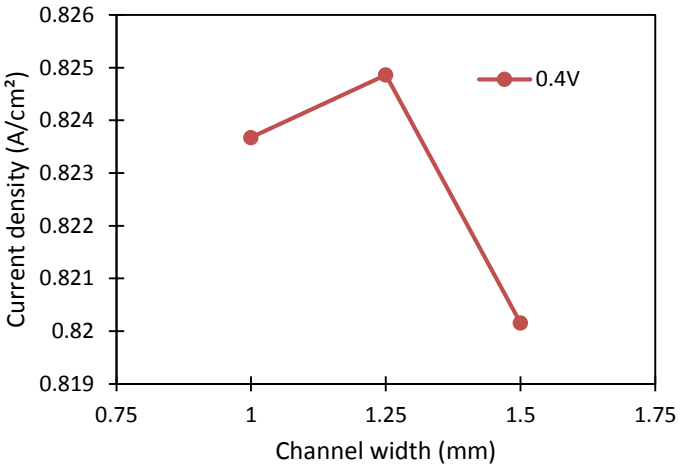

Fig. 7. Graph of current density at 0.4 V with variations in channel width on biometric flow field.

Figure 8 shows the pressure drop as a function of different channel widths. The wider the channel, the lower the pressure drop. Pressure drop for biometric flow fields with 1.25 mm channel width that is 53.51 Pa. In other cases, the simulation results for parallel flowfield show a pressure drop of 486.91 Pa. This shows that the pressure drop for biometric flow fields is only 11% of the parallel flow field. Figure 9 shows the oxygen concentration at the cathode catalyst surface. The wider the channel, the greater the oxygen concentration. The 1.25 mm channel width has an adequate pressure drop and sufficient flow mass, resulting in good current density at the medium voltage (0.4 V) and low voltage (0.2 V). In addition, the number of ribs on the 1.5 mm channel width is less than the number of ribs on the 1.25 mm channel width. The small amount of rib causes a reduction in the electron channel between the gas diffusion layer and the current collector, this will affect ohmic barriers [5, 8].

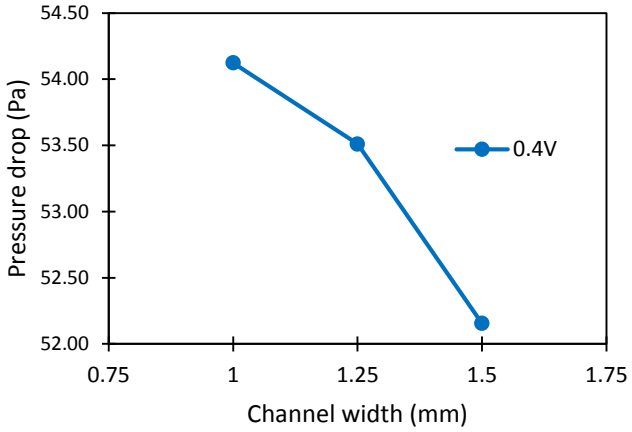

Fig. 8. Effect of channel width on pressure drop on 0.4 V on biometric flow field.

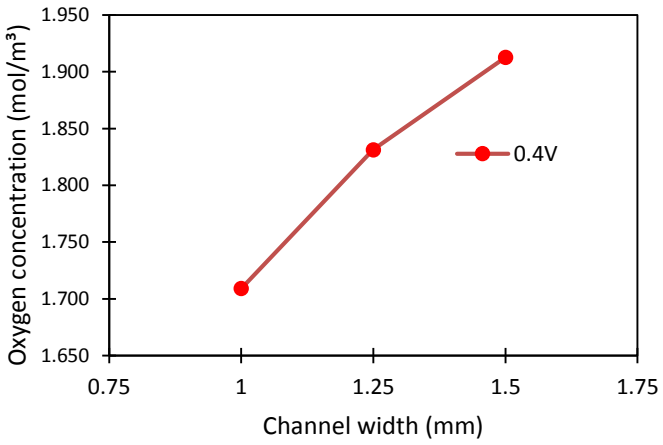

Fig. 9. Effect of channel width on oxygen concentration at 0.4 V on biometric flow field.

In Fig. 10, we can see that the current density for channel width 1.25 mm higher than channel width 1 mm and 1.5 mm at low voltage. Differences are seen when compared to medium voltage conditions. At 1.5 mm channel width, the resulting current density is higher than the channel width of 1 mm. This is because, at low voltages, the oxygen concentration gives a greater influence than the oxygen pressure to the diffusion layer [9].

From Fig. 11, we can see that the peak power density for parallel flow fields is 0.27 W/cm², while for biometric flow fields is 0.33 W/cm². Therefore, power density for biometric flow fields is 22% is higher when compared to the parallel flow fields on the cathode side. The amount of power density produced is directly proportional to current density, therefore, the increase in power density is also caused by an increase in uniform distribution of oxygen supply on the cathode side.

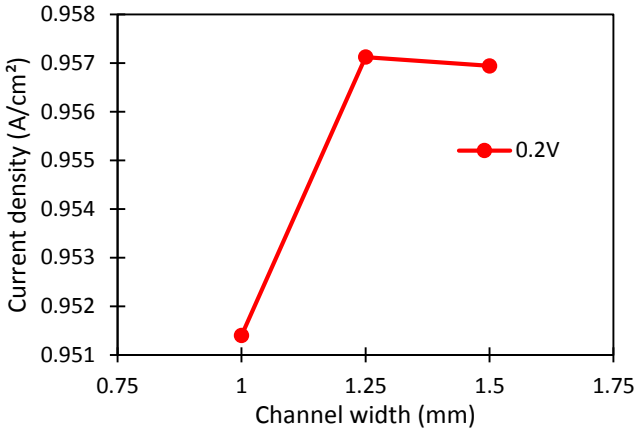

Fig. 10. Current density graph at 0.2 V with variations in channel width on biometric flow field.

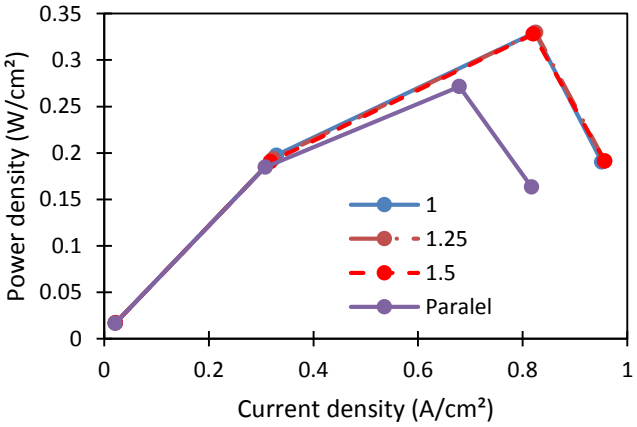

Fig. 11. Power density graph with variations in flow fields.

4. Conclusions

From this study, it can be concluded that the use of biometric flow fields produces a higher power density of 22% when compared with the use of parallel flow fields on the cathode side. This is because the distribution of oxygen supply in the biometric flow field is more uniform, therefore, it can meet the oxygen demand on the cathode catalyst. In addition, biometric flow fields have lower pressure drop advantages, only 11% of parallel flow fields.

Nomenclatures

A	Area, m²
F	Faraday constant, 9.65.107 C/kmol
j^{ref}	Reference exchange current density per active surface area, A/m²
R	Ideal gas constant, 8.314 J/kmol
R_a, R_c	Electrical current anode side and cathode side, A/m³
R_s, R_m	Electrical current solid phase and membrane phase, A/m³
S_φ	Source term transported quantity
$\overline{u}$	Velocity average, m/s
$\vec{V}$	Velocity vector, m/s
V_{oc}	Open circuit voltage, volts

Greek Symbols

∇	Del operator
α_a, α_c	Anode and cathode transfers coefficients
Γ_φ	Diffusivity of transported quantity, m²/s
γ_a, γ_c	Anode and cathode concentration exponents
γ	Gamma uniformity index
ζ	Specific active surface area, 1/m
η_a, η_c	Anode and cathode overpotentials
ρ	Mixture density, kg/m³
σ_s, σ_m	Electrical conductivity solid phase and membrane phase, 1/ohm m
φ	Transported quantity (mass, momentum, energy)
ϕ_s, ϕ_m	Electric potential solid phase and membrane phase, volts

Abbreviations

3D	Three Dimensional
DMFC	Direct Methanol Fuel Cell
ITS	Institut Teknologi Sepuluh Nopember
LPPM	Lembaga Penelitian dan Pengabdian Masyarakat
PEMFC	Polymer Electrolyte Membrane Fuel Cell
PTFE	Polytetrafluoroethylene

Acknowledgement

The authors acknowledge Lembaga Penelitian dan Pengabdian Masyarakat Institut Teknologi Sepuluh Nopember (LPPM-ITS) Indonesia for funding this research work through grants Penelitian Laboratorium Dana Lokal ITS 2018.

References

1. Maslan, N.H.; Gau, M.M.; Masdar, M.S.; and Rosli, M.I. (2016). Simulation of porosity and PTFE content in gas diffusion layer on Proton exchange membrane fuel cell performance. *Journal of Engineering Science and Technology* (*JESTEC*), 11(1), 85-95.
2. Hadjadj, R.; and Kaabar, W. (2018). Numerical investigation of flow field in Proton exchange membrane fuel cell at different channel geometries. *Journal of Engineering Science and Technology* (*JESTEC*), 13(4), 1070-1089.
3. Li, X.; and Sabir, I. (2005). Review of bipolar plates in PEM fuel cells: Flow-field designs. *International Journal of Hydrogen Energy*, 30(4), 359-371.
4. Manso, A.P.; Marzo, F.F.; Barranco, J.; Garikano, X.; and Mujika, M.G. (2012). Influence of geometric parameters of the flow fields on the performance of a PEM fuel cell. A review. *International Journal of Hydrogen Energy*, 37(20), 15256-15287.
5. Chowdhury, M.Z.; Genc, O.; and Toros, S. (2018). Numerical optimization of channel to land width ratio for PEM fuel cell. *International Journal of Hydrogen Energy*, 43(23), 10798-10809.
6. Ramesh, P.; Dimble, S.S.; Duttagupta, S.P.; and Agarwal, V. (2011). Effect of segmented contacts on fuel cell performance using 3-D modeling. *Proceedings of the International Conference on Energy and Electrical Systems (ICEES).* Kuala Lumpur, Malaysia.
7. Kreesaeng, S.; Chalermsinsuwan, B.; and Piumsomboon, P. (2015). Effect of channel designs on open-cathode PEM fuel cell performance: A computational study. *Energy Procedia*, 79, 733-745.
8. Muthukumar, M.; Karthikeyan, P.; Vairavel, M.; Loganathan, C.; Praveenkumar, S.; and Senthil Kumar, A.P. (2014). Numerical studies on PEM fuel cell with different landing to channel width of flow channel. *Procedia Engineering*, 97, 1534-1542.
9. Currie, J.M. (2010). *Biomimetic design applied to the redesign of a pem fuel cell flow field*. Master Thesis. Mechanical and Industrial Engineering, University of Toronto, Toronto, Kanada.
10. Lim, B.H.; Majlan, E.H.; Daud, W.R.W.; Rosli, M.I.; and Husaini, T. (2017). Numerical analysis of modified parallel flow field designs for fuel cells. *International Journal of Hydrogen Energy*, 42(14), 9210-9218.
11. Ozden, A.; Ercelik, M.; Ouellette, D.; Colpan, C.O.; Ganjehsarabi, H.; and Hamdullahpur, F. (2017). Designing, modeling and performance investigation of bio-inspired flow field based DMFCs. *International Journal of Hydrogen Energy*, 42(33), 21546-21558.
12. Guo, N.; Leu, M.C.; and Koylu, U.O. (2014). Bio-inspired flow field designs for polymer electrolyte membrane fuel cells. *International Journal of Hydrogen Energy*, 39(36), 21185-21195.
13. Roshandel, R.; Arbabi, F.; and Moghaddam, G.K. (2012). Simulation of an innovative flow-field design based on a bio inspired pattern for PEM fuel cells. *Renewable Energy*, 41, 86-95.

14. Kloess, J.P.; Wang, X.; Liu, J.; Shi, Z.; and Guessous, L. (2009). Investigation of bio-inspired flow channel designs for bipolar plates in Proton exchange membrane fuel cells. *Journal of Power Sources*, 188(1), 132-140.
15. Arvay, A.; French, J.; Wang, J.-C.; Peng, X.-H.; and Kannan, A.M. (2015). Modeling and simulation of biologically inspired flow field designs for Proton exchange membrane fuel cells. *The Open Electrochemistry Journal*, 6, 1-9.
16. Heidary, H.; Kermani, M.J.; Prasad, A.K.; Advani, S.G.; and Dabir, B. (2017). Numerical modelling of in-line and staggered blockages in parallel flowfield channels of PEM fuel cells. *International Journal of Hydrogen Energy*, 42(4), 2265-2277.
17. Iranzo, A.; Muñoz, M.; Rosa, F.; and Pino, J. (2010). Numerical model for the performance prediction of a PEM fuel cell. Model results and experimental validation. *International Journal of Hydrogen Energy*, 35(20), 11533-11550.
18. Limjeerajarus, N.; and Charoen-amornkitt, P. (2015). Effect of different flow field designs and number of channels on performance of a small PEFC. *International Journal of Hydrogen Energy*, 40(22), 7144-7158.
19. ANSYS. (2013). *ANSYS fluent fuel cell modules manual*. Canonsburg, Pennsylvania: ANSYS, Inc.
20. Nassau, C.J.; and Agarwal, R.K. (2018). Curvature effects and flow uniformity optimization of a blood microchannel. *Mechanical Engineering and Materials Science Independent Study*, 71, 8 pages.
21. Chang, D.-H.; and Wu, S.-Y. (2015). The effects of channel depth on the performance of miniature proton exchange membrane fuel cells with serpentine-type flow fields. *International Journal of Hydrogen Energy*, 40(35), 11659-11667.
22. Fahruddin, A.; Ichsani, D.; and Taufany, F. (2018). Improving PEM fuel cell performance using in-line triangular baffles in triple serpentine flow field. *MATEC Web of Conferences*, 197, 08010.
23. Lim, B.H.; Majlan, E.H.; Daud, W.R.W.; Rosli, M.I.; and Husaini, T. (2017). Numerical analysis of modified parallel flow field designs for fuel cells. *International Journal of Hydrogen Energy*, 42(14), 9210-9218.
24. McCabe, W.L.; Smith, J.C.; and Harriott, P. (2005). *Unit operations of chemical engineering* (7th ed.). New York, United States of America: McGraw-Hill.